Thomas, M.; Dobslaw, H.; Stuck, J.; Seitz, F.: The ocean's contribution to polar motion excitation - as many solutions as numerical models?

In: Plag, H.-P.; Chao, B.; Gross, R.; van Dam, T. (eds.) Forcing of polar motion in the Chandler frequency band: A contribution to understanding interannual climate variations, Cahiers du Centre Européen de Géodynamique et de Séismologie, Vol. 24, pp 143-148, European Center for Geodynamics and Seismology (ECGS), ISBN (Print) 2-9599804-1-7, 2005.

In: Forcing of Polar Motion in the Chandler Frequency Band: A Contribution to Understanding Interannual Climate Variations, H.-P. Plag et al (Eds.), Cahiers du Centre Européen de Géodynamique et de Séismologie, Vol. 24, 143-148, Luxembourg

The ocean's contribution to polar motion excitation - as many solutions as numerical models?

M. Thomas, H. Dobslaw
Institut für Planetare Geodäsie, Technische Universität Dresden, Mommsenstr. 13, D-01062 Dresden, Germany, e-mail: mthom@rcs.urz.tu-dresden.de

J. Stuck
GeoForschungsZentrum Potsdam, Telegrafenberg, D-14473 Potsdam, Germany

F. Seitz
Deutsches Geodätisches Forschungsinstitut, Marstallplatz 8, D-80539 München, Germany

Abstract. By analysing realtime model runs performed with the Ocean Model for Circulation and Tides over several decades with different forcing conditions, the impact of various components of ocean dynamics, i.e., the thermohaline, wind-, and pressure driven circulation as well as long-period tides, and secondary effects arising from loading and self-attraction on polar motion excitation is estimated. From resulting effective angular momentum functions power spectral densities are calculated and contrasted with corresponding results of other numerical ocean models provided at the Special Bureau for the Oceans at the Global Geophysical Fluids Center. After superimposition with corresponding atmospheric effects it turns out that the atmospheric-oceanic model combinations NCEP/MIT, NCEP/ECCO, and ECHAM3/OMCT lead to similar excitation power in the Chandler frequency band which always exceeds the observed power.

1 Introduction

Since oceanic in situ data are temporary and regional, i.e., restricted in time and space, and satellite data are essentially confined to the sea surface, numerical ocean models provide an indispensable tool for estimations of the ocean's contribution to variations of global parameters of the Earth, e.g., the Earth orientation parameters. In recent years several numerical global ocean models have been applied in order to examine the role of the oceans with respect to the excitation of polar motion on hourly up to decadal timescales, in particular with respect to the excitation of the Chandler wobble. However, the ocean models that have been used to estimate corresponding oceanic angular momentum (OAM) strongly differ, e.g., with respect to time-space resolution, model physics, and forcing conditions. Besides, they commonly use different numerical parameterizations to reproduce similar dynamical processes. Thus, varying model concepts reproduce different components of ocean dynamics, and one has to beware of comparing not comparable results.

Ponte et al. (1998) and Ponte and Stammer (1999) showed by means of the near-global baroclinic general circulation model of the Massachusetts Institute of Technology (MIT) (Marshall et al., 1997a, 1997b) driven with twice-daily wind stresses, daily heat and freshwater fluxes from NCEP/NCAR reanalysis data (Kalnay et al., 1996) that the oceanic thermohaline and wind-driven circulation plays an important role for polar motion excitation on annual to submonthly timescales. Gross (2000a) used the same OAM time series and corresponding time series of atmospheric angular momentum computed from the NCEP/NCAR reanalysis project to estimate the importance of atmospheric and oceanic mass redistributions with respect to the excitation of the Chandler wobble during 1985-1996. Johnson et al. (1999) discussed the influence of the thermal and wind-driven circulation with respect to polar motion excitation resulting from simulations with the Parallel Ocean Climate Model (POCM) (Semtner and Chervin, 1992) driven with monthly mean heat fluxes and 3-daily wind stresses provided by the European Centre for Medium-Range Weather Forecasts.

More recently, Gross et al. (2003) used output from an ocean model of the Estimating the Cir-

culation and Climate of the Ocean (ECCO) consortium, which is based on the MIT model and was also driven by atmospheric NCEP/NCAR reanalysis data, to analyse 21 years long OAM series representing the influence of the thermohaline and wind-driven circulation with respect to the excitation of polar motion from terannual to interannual timescales. In contrast to the above-named model studies, Ponte et al. (2001) estimated OAM series by constraining the model to oceanic data. However, the investigations mentioned so far exclusively consider thermohaline and wind-driven components of oceanic circulation. Thomas et al. (2001) and Seitz et al. (2004) included additional effects due to the pressure-driven circulation, i.e., deviations from a pure inverse barometric response of the ocean's surface to atmospheric pressure changes, as well as secondary influences arising from loading and self-attraction (LSA) of a baroclinic water column; further, sea-ice dynamics and nonlinear interactions between various components of ocean dynamics were taken into account.

In the following, the impact of such so-called second-order effects in the global ocean on the excitation of polar motion on timescales from months to decades is estimated by means of simulations with a baroclinic global ocean model for circulation and tides. The resulting oceanic excitations are contrasted with numerical oceanic solutions provided at the Special Bureau for the Oceans (SBO) at the Global Geophysical Fluids Center (GGFC) (Chao et al., 2000). After superimposition with corresponding atmospheric excitations they are compared with observed geodetic excitations in the time and frequency domain.

2 Models and data

The Ocean Model for Circulation and Tides (OMCT) (Thomas et al., 2001) used here is based on nonlinear balance equations for momentum, the continuity equation of an incompressible fluid, and conservation equations for heat and salt. Implemented is a sea-ice model (Hibler, 1979), and effects due to LSA are taken into account by means of a secondary potential proportional to the mass in the local water column (cf., Thomas et al, 2001). Thirteen layers exist in the vertical, the horizontal resolution is 1.875° in longitude and latitude, and the temporal resolution is 30 minutes.

For the period 1949-1994 the ocean model

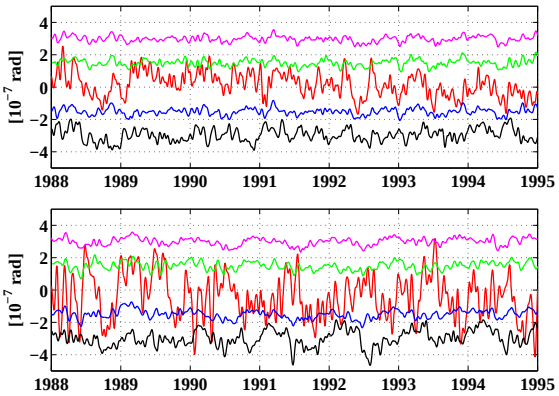

Figure 1: Effective angular momentum functions χ_1 (upper panel) and χ_2 (lower panel). Geodetic excitations according to the EOP C04 data of the IERS (red) are contrasted with thermohaline, wind-driven oceanic contributions resulting from simulations with the MIT model (Ponte et al., 1998) (magenta), POCM (Johnson et al., 1999) (green), ECCO (Gross et al., 2003) (blue), and OMCT (black). All time series have been arbitrarily shifted.

was driven with twice-daily atmospheric forcing fields from the global general circulation model ECHAM3 (DKRZ, 1992; Roeckner et al., 1992) including surface temperatures, freshwater fluxes, wind-stresses, and atmospheric surface pressure. The corresponding dynamical state of the ECHAM3 atmosphere results from simulations that were forced with monthly means of observed sea surface temperatures and global ice coverage according to the GISST data set provided by the Hadley Center for Climate Prediction and Research (Bracknell) (Parker et al., 1994).

3 Polar motion excitation

3.1 Effective angular momentum functions

From instantaneous mass distributions and currents corresponding OAM time series are calculated and transformed to effective angular momentum (EAM) functions, $\chi_{1,2}$, using the formulation of Barnes et al. (1983). χ_1 is orientated to the meridian of Greenwich, χ_2 to $90°E$ respectively. Since only variations with periods longer than a month are considered here, calculated EAM functions are low-pass filtered with a cutoff period of 30 days. In Figure 1, low-pass filtered time series $\chi_{1,2}$ resulting from OMCT simulations of the thermohaline, wind-driven circulation alone are contrasted with cor-

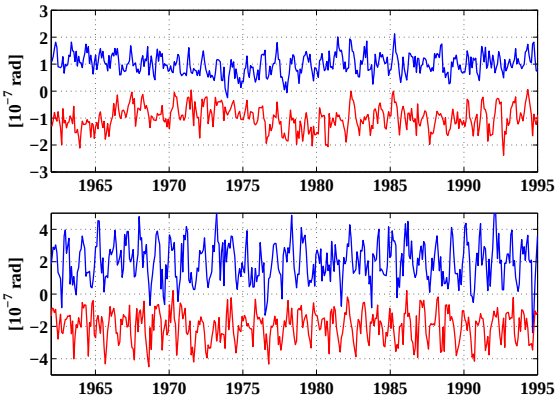

Figure 2: EAM functions χ_1 (blue) and χ_2 (red) resulting from OMCT simulations of the thermohaline, wind-driven circulation (upper panel) and the pressure-driven circulation (lower panel).

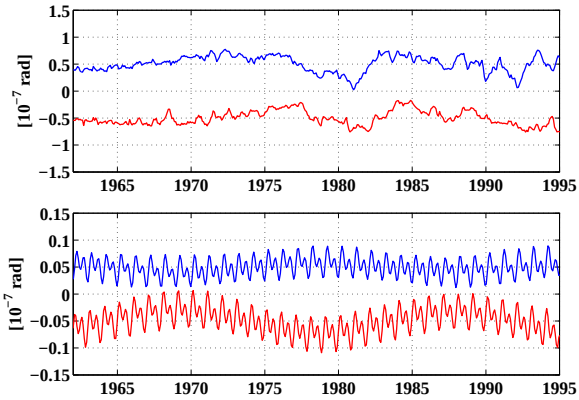

Figure 3: EAM functions χ_1 (blue) and χ_2 (red). In the upper panel contributions of loading and self-attraction, in the lower panel excitations due to long-period tides are given.

responding oceanic excitations provided at the SBO at the GGFC. Obviously, excitations resulting from ECCO (Gross et al., 2003) and MIT (Ponte et al., 1998) simulations nearly coincide, since the ECCO model is based on the MIT model and both simulations were driven with NCEP/NCAR reanalysis data. The latter results are quite similar to POCM excitations (Johnson et. al, 1999), what might be a consequence of resemblances concerning atmospheric forcing conditions, too. In contrast to the excitations resulting from the models POCM, MIT, and ECCO, which apply reanalysis data, the OMCT simulation was driven with data of the unconstrained ECHAM model. Thus, it stands to reason that comparatively high excitations from OMCT simulations have mainly to be ascribed to differences in atmospheric forcing conditions.

According to Figure 2, oceanic contributions due to atmospheric pressure alone clearly exceed thermohaline, wind-driven effects. However, a significant part of pressure-induced excitations will be compensated when atmospheric excitations are superimposed, since the ocean's response to atmospheric pressure changes is nearly inverse barometric on timescales longer than a few days. Polar motion excitations due to loading and self-attraction of a baroclinic water column are most pronounced on interannual timescales whereas annual variations are generally one order of magnitude less than thermohaline, wind-driven effects (Fig. 3). However, so-called secondary effects arising from LSA exceed excitations caused by primary long-period tides.

In Figure 4 time series $\chi_{1,2}$ resulting from the simultaneous model run are depicted, which contain the effects of the thermohaline, wind-, and pressure-driven circulation, long-period tides as well as secondary effects due to LSA, sea-ice, and nonlinear interactions. Oceanic and corresponding atmospheric excitations calculated from ECHAM3 forcing data are nearly out of phase, mainly as a consequence of atmospheric pressure coupling. Thus, it is not surprising that significant contributions are compensated when atmospheric and oceanic signals are superimposed (black lines). To get an impression of the quality of the numerical results, observed polar motion data made available by the International Earth Rotation Service (IERS, 1997) (EOP C 04 data set) were transformed to corresponding geodetic excitation functions by applying the deconvolution method of Wilson (1985). According to Wilson and Vicente (1990) a Chandler period of 433.0 sidereal days and a damping factor $Q = 179$ were assumed. Exemplarily, for the time interval 1985-1995 in Figure 5 geodetic excitations are contrasted with simulated excitations containing the combined atmospheric and oceanic contributions. Although the numerical simulations, in particular with respect to χ_1, tend to overestimate the excitations, typical characteristics of the observed signals are well reproduced. The qualitative agreement of the unconstrained model results and geodetic observations indicates that the applied numerical models are capable of describing atmospheric and oceanic transient dynamics (i.e., currents as well as mass redistributions) quite realistic in an inte-

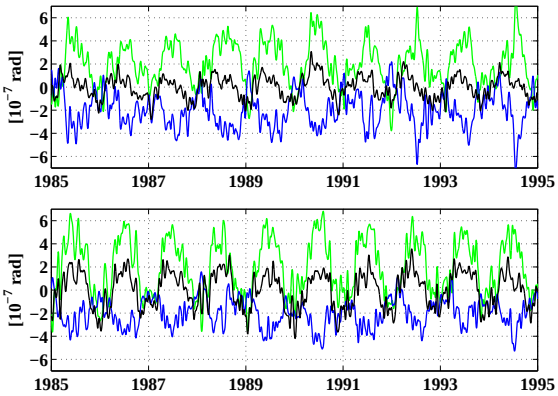

Figure 4: EAM functions χ_1 (upper panel) and χ_2 (lower panel) resulting from a simultaneous run of oceanic circulation and tides (blue) and from atmospheric wind and pressure variations (green). The black lines represent combined atmospheric and oceanic excitations.

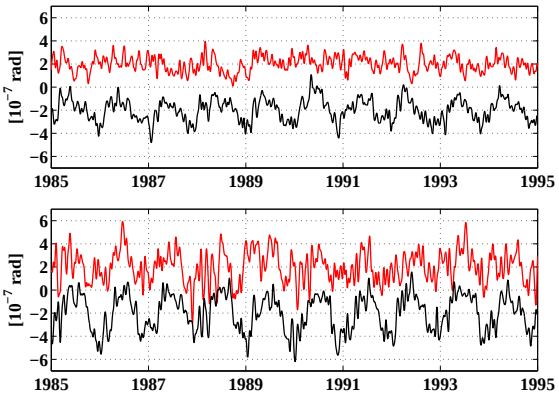

Figure 5: Geodetic EAM functions (red) according to the EOP C 04 data of the IERS and combined atmospheric-oceanic EAM functions resulting from ECHAM3 and OMCT simulations (black). In the upper panel time series χ_1, in the lower panel time series χ_2 are depicted.

gral manner. However, this optimistic valuation has always to be seen against the background of a pure theoretical model approach.

3.2 Power spectral density

By means of the multitaper method, power spectral densities (PSD) are calculated from EAM time series $\chi_{1,2}$. In the upper panel of Figure 6 the prograde component of geodetic excitation derived from EOP C 04 data is contrasted with corresponding prograde components derived from various simulated oceanic excitations including effects of currents and mass redistributions due to the thermohaline and wind-driven circulation. In accordance with time series $\chi_{1,2}$ depicted in Figure 1, OMCT excitations yield generally higher power spectral densities than the MIT model (Ponte et al., 1998), POCM (Johnson et al., 1999), and ECCO (Gross et al., 2003), especially with respect to annual variations. However, since the overlapping period 1988 to 1995 is too short for comparing statistical analysis, the power spectral densities of various oceanic excitations had to be calculated for different time intervals (cf. introduction), thus, the comparability is restricted.

In the lower panel of Figure 6 the prograde PSD component computed from the simultaneous OMCT run of circulation and tides, from the ECHAM3 result, and from the superimposed signal of ECHAM3 and OMCT is depicted. Since the OMCT simulation was also forced with atmospheric pressure variations and consequently no inverse barometric correction had to be applied to ECHAM3, significant power is compensated after superimposition of ECHAM3 and OMCT indicating that the ocean's response to atmosheric pressure is close to that of an inverted barometer on long timescales.

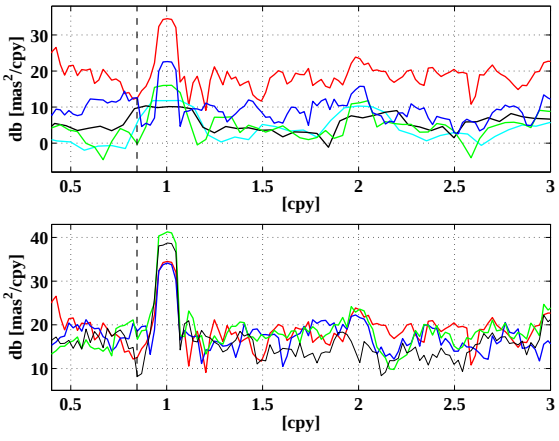

Figure 6: Prograde components of power spectral density (PSD). In the upper panel PSDs from oceanic simulations of the thermohaline, wind-driven circulation are contrasted: MIT model (cyan), POCM (black), ECCO (green), OMCT (blue). In the lower panel PSDs of the simultaneous OMCT run of circulation and tides (blue), the ECHAM3 simulation (green), and the combined ECHAM3/OMCT signal (black) are shown. Red lines represent the PSD as derived from EOP C 04 data.

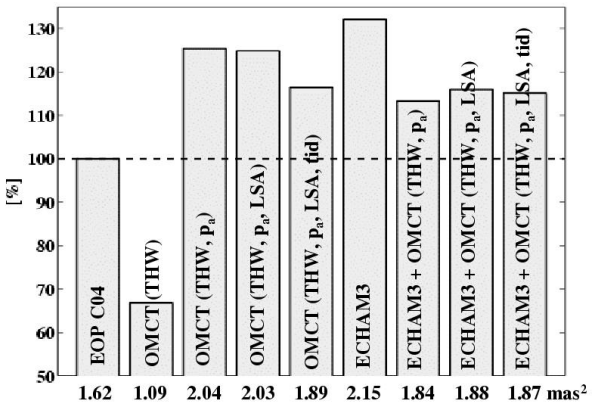

Figure 7: Chandler band excitation power. Comparison of observed power calculated from EOP C 04 with oceanic contributions due to thermohaline, wind-driven effects (THW), pressure-driven circulation (p_a), LSA, and tides and corresponding combined oceanic and atmospheric excitation power. Shown is the sum of contributions from motions and mass redistributions.

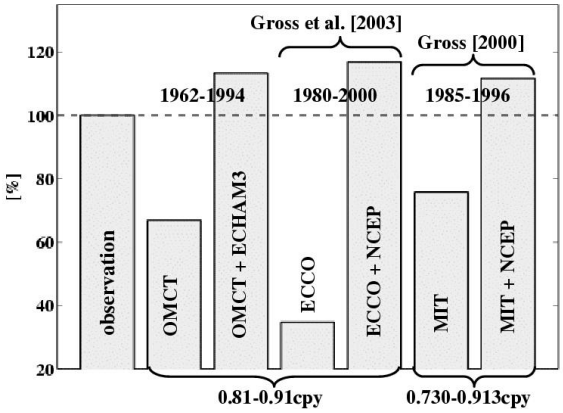

Figure 8: Chandler band excitation power. Oceanic and combined oceanic-atmospheric excitation power provided by various models. Please note different time intervals and Chandler frequency bands. Oceanic power calculated from ECCO and MIT model exclusively take into account thermohaline, wind-driven effects; OMCT additionally considers the pressure-driven circulation.

3.3 Chandler band excitation power

In anology to Gross (2000a) and Gross et al. (2003), finally, the power in the Chandler band is estimated by integration of the PSD (Figure 6) across the Chandler frequency band. Here, the frequency band was assumed to range between 0.81 and $0.91cpy$. As shown in Figure 7, the ocean's thermohaline, wind-driven circulation provides about 68% of observed power. Since atmospheric pressure forcing was included, pressure-driven oceanic effects and atmospheric contributions located over oceanic areas compensate when oceanic and atmospheric contributions are superimposed. Only slightly modifications of excitation power have to be stated due to the consideration of LSA. The inclusion of long-period tides generally reduces total excitation power.

To compare the Chandler band excitation power provided by ECHAM3/OMCT with corresponding power calculated from the model combinations NCEP/MIT (Gross, 2000a) and NCEP/ECCO (Gross et al., 2003) the relative importance of oceanic and atmospheric excitation power with respect to the observation is depicted in Figure 8. According to Gross (2000a), who computed the excitation power in the frequency band $0.730 - 0.913cpy$ resulting from NCEP/MIT and SPACE97 (Gross, 2000b), the total atmospheric plus oceanic excitation power is equivalent to 112% of the observed power. Analogously, following Gross et al. (2003), in the frequency band $0.81 - 0.91cpy$ the excitation power deduced from NCEP/ECCO is 117% of the observed power calculated from COMB2000 (Gross, 2001). In contrast to NCEP/MIT and NCEP/ECCO, the model combination ECHAM3/OMCT additionally takes into account the pressure-driven circulation, i.e., deviations from a purely inverse barometric response of the ocean's surface to atmospheric pressure variations. In the frequency band $0.81 - 0.91cpy$ the excitation power of ECHAM3/OMCT exceeds the observed power calculated from EOP C 04 by 13%. Thus, although the calculations refer to different periods and slightly distinct Chandler frequency bands and are based on various model concepts, e.g., unconstrained and analysis models of the atmosphere, the atmospheric-oceanic model combinations provide astonishing similar excitation power. However, significant differences have to be stated with respect to pure oceanic excitation in the Chandler frequency band, since the ECCO simulation suggests less than half as much excitation power than the MIT model and OMCT.

4 Conclusions

The comparison of EAM functions due to thermohaline and wind-driven effects predicted by

various global ocean models turns out that OMCT provides slightly higher variations than POCM, MIT, and ECCO what mainly has to be attributed to differences with respect to atmospheric forcing conditions. While the POCM, ECCO, and MIT model were driven by reanalysis data, the OMCT was forced by climate data. The simultaneous calculation of circulation and tides suggests additional polar motion excitations caused by LSA and long-period tides which are generally one order of magnitude less than thermohaline and wind-driven contributions. Accordingly, with respect to the Chandler band excitation power in the frequency band $0.81 - 0.91 cpy$ these second-order effects are detectable, but marginally reflected.

Despite significant conceptional differences concerning parameterizations and model physics taken into account and applied atmospheric forcing conditions, the predictions of Chandler band excitation power by the model combinations MIT/NCEP, ECCO/NCEP, and ECHAM3/OMCT are in surprisingly good agreement, suggesting that atmospheric plus oceanic excitation power exceed observations in the range of 12% to 17%.

Acknowledgements

We thank the Deutsche Klimarechenzentrum, Hamburg, Germany, for providing data from the ECHAM3-T21 simulations.

References

Barnes, R. T. H., R. Hide, A. A. White, and C. A. Wilson, Atmospheric angular momentum fluctuations, length-of-day changes and polar motion, *Proc. R. Soc. Lond.*, A 387, 31, 1983.

Chao, B. F., V. Dehant, R. S. Gross, R. D. Ray, D. A. Salstein, M. M. Watkins, and C. R. Wilson, Space geodesy monitors mass transports in global geophysical fluids, *Eos Trans. AGU, 81*, 247-250, 2000.

Deutsches Klimarechenzentrum (DKRZ) Modellbetreuungsgruppe, The ECHAM3 atmospheric general circulation model, *Tech. Rep. No. 6, ISSN 0940-9237*, 184 pp., Deutsches Klimarechenzentrum, Hamburg, Germany, 1992.

Gross, R. S., The excitation of the Chandler wobble, *Geophys. Res. Lett., 27*, 2329-2332, 2000a.

Gross, R. S., Combinations of Earth orientation measurements: SPACE97, COMB97, and POLE97, *J. Geodesy*, vol.73, pp. 627-637, 2000b.

Gross, R. S., Combinations of Earth orientation measurements: SPACE2000, COMB2000, and POLE2000, *JPL Publ., 01-2*, 25 pp., 2001.

Gross, R. S., I. Fukumori, and D. Menemenlis, Atmospheric and oceanic excitation of the Earth's wobbles during 1980-2000, *J. Geophys. Res., 108*,(B8), 2370, doi:10.1029/2002JB002143, 2003.

Hibler III, W. D., A dynamic thermodynamic sea ice model, *J. Phys. Oceanogr., 9*, 815-846, 1979.

International Earth Rotation Service (IERS), *1997 IERS Annual Report*, Observ. de Paris, Paris, France, 1997.

Johnson, T. J., C. R. Wilson, and B. F. Chao, Oceanic angular momentum variability estimated from the Parallel Ocean Climate Model, 1988-1998, *J. Geophys. Res., 104*, 25183-25195, 1999.

Kalnay, E., M. Kanamitsu, R. Kistler, W. Collins, D. Deaven, L. Gandin, M. Iredell, S. Saha, G. White, J. Woollen, Y. Zhu, M. Chelliah, W. Ebisuzaki, W. Higgins, J. Janowiak, K.C. Mo, C. Ropelewski, J. Wang, A. Leetmaa, R. Reynolds, R. Jenne, and D. Joseph, The NCEP/NCAR 40-year reanalysis project, *Bull. Am. Meteorol. Soc., 77*, (3), 437-471, 1996.

Marshall, J., C. Hill, L. Perelman, and A. Adcroft, Hydrostatic, quasi-hydrostatic, and nonhydrostatic ocean modelling, *J. Geophys. Res., 102*, 5733-5752, 1997a.

Marshall, J., A. Adcroft, C. Hill, L. Perelman, and C. Heisey, A finite-volume, incompressible Navier Stokes model for studies of the ocean on parallel computers, *J. Geophys. Res., 102*, 5753-5766, 1997b.

Parker, D. E., P. D. Jones, C. K. Folland, and A. Bevan, Interdecadal changes of surface temperature since the late nineteenth century, *J. Geophys. Res., 99*, 14373-14399, 1994.

Ponte, R. M., D. Stammer, and J. Marshall, Oceanic signals in observed motions of the Earth's pole of rotation, *Nature, 391*, 476-479, 1998.

Ponte, R. M., and D. Stammer, Role of ocean currents and bottom pressure variability on seasonal polar motion, *J. Geophys. Res., 104*, 23393-23409, 1999.

Ponte, R. M., D. Stammer, and C. Wunsch, Improving ocean angular momentum estimates using a model constrained by data, *Geophys. Res. Lett., 28*, 1775-1778, 2001.

Roeckner, E., K. Arpe, L. Bengtsson, S. Brinkop, L. Dümenil, M. Esch, E. Kirk, F. Lunkeit, M. Ponater, B. Rockel, R. Sausen, U. Schlese, S. Schubert, and M. Windelband, Simulation of the present-day climate with the ECHAM model: impact of the model physics and resolution, *Techn. Rep. No. 93*, Max-Planck-Institut für Meteorologie, Hamburg, 1992.

Seitz, F., J. Stuck, and M. Thomas, Consistent atmospheric and oceanic excitation of the Earth's free polar motion, *Geophys. J. Int.*, 157, 25-35, 2004.

Semtner, A. J., and R. M. Chervin, Ocean general circulation from a global eddy-resolving (primitive equation) model (POCM), *J. Geophys. Res., 97*, 5493-5550, 1992.

Thomas, M., J. Sündermann, and E. Maier-Reimer, Consideration of ocean tides in an OGCM and impacts on subseasonal to decadal polar motion excitation, *Geophys. Res. Lett., 28*, 12, 2457-2460, 2001.

Wilson, C. R., Discrete polar motion equations, *Geophys. J. Roy. astr. Soc.*, 80, 551-554, 1985.

Wilson, C. R., and R. O. Vicente, Maximum likelihood estimates of polar motion parameters, in *Variations in Earth Rotation, Geophys. Monogr. Ser.*, vol. 59, edited by D. D. McCarthy and W. E. Carter, pp. 151-155, AGU, Washington, D. C., 1990.